LA-9401-MS

Los Alamos National Laboratory is operated by the University of California for the United States Department of Energy under contract W-7405-ENG-36.

Current Diffusion in Rail-Gun Conductors

Los Alamos
Los Alamos National Laboratory
Los Alamos, New Mexico 87545

Edited by Eleanor Langley, Group WX-4

LA-9401-MS

UC-38
Issued: June 1982

Current Diffusion in Rail-Gun Conductors

J. F. Kerrisk

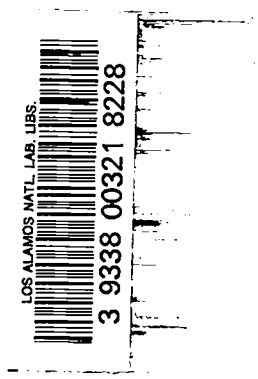

Los Alamos National Laboratory
Los Alamos, New Mexico 87545

CURRENT DIFFUSION IN RAIL-GUN CONDUCTORS

by

J. F. Kerrisk

ABSTRACT

A method has been developed to analyze one- and two-dimensional, nonlinear current diffusion in rail-gun conductors. A nonlinear current-diffusion equation that accounts for the temperature dependence of electrical conductivity has been developed from Maxwell's equations. A finite-difference heat-transfer computer program was adapted to solve the current-diffusion and thermal-diffusion problems for rail-gun conductors in one and two dimensions. The nonlinear current-diffusion equation was also extended to account for the magnetic-field dependence of the magnetic permeability, thus allowing ferromagnetic materials to be considered. A one-dimensional finite-difference technique was developed for ferromagnetic materials. Two one-dimensional test problems that compare results with other analyses are discussed. A series of calculations of current density and rail temperature was done for various size rectangular rails. One analysis of current diffusion in a ferromagnetic material was also performed.

I. INTRODUCTION

Rail guns or electromagnetic accelerators are devices that accelerate projectiles by the interaction of an electric current and a magnetic field.[1,2] These devices offer the possibility of producing very high velocities, much higher than are attained in conventional gas-driven guns. Indeed, experiments have shown that it is possible to electromagnetically accelerate projectiles of a few grams to 10 km/s; considerably higher velocities appear to be attainable. One of the problems encountered in the design of rail guns is the high current flow (megaamperes) and high magnetic fields employed. Although these conditions exist for only a short time (milliseconds), rail-gun conductors can be damaged from joule heating or from magnetic forces. This report describes a method that can be used to analyze current diffusion and thermal diffusion in rail-gun conductors. These analyses are necessary to predict rail damage from joule heating.

Physically, a rail gun is usually made of two long, parallel conductors. The projectile starts at the breech end, at rest or with some initial velocity (see Fig. 1). Current flows into one rail at the breech end, between rails in an armature behind the projectile (or possibly through the projectile), and out of the other rail at the breech end. Both solid metallic armatures and plasma armatures (arcs) have been used in rail guns. The interaction of the current flow through

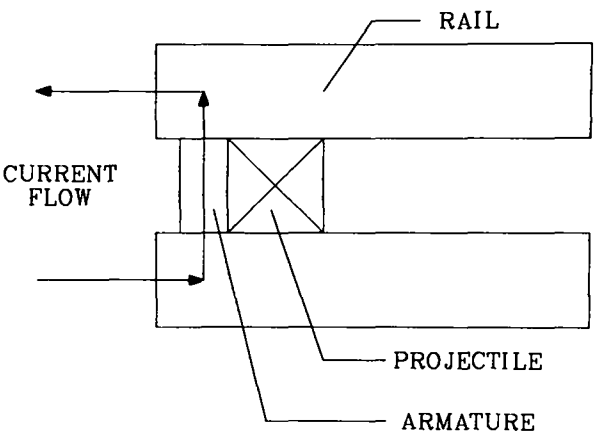

Fig. 1. Schematic diagram of a rail gun.

the armature with the magnetic field associated with the current flow in the rails accelerates the projectile toward the muzzle. As is evident from Fig. 1, current flows in the breech during the entire acceleration; no current flows in the rails in front of the armature. Thus, near the muzzle, current flow will occur only at the end of the acceleration.

At any axial location along the rails, current will start to flow in the rail cross section as the projectile passes. Figure 2 shows an example of two rails with rectangular cross section (in the x-y plane); the rails are assumed to be long in the z-direction (perpendicular to the paper). Current flow is in the z-direction only; however, the current density is a function of x and y. Initially, the current is distributed over a thin layer near the surface of each conductor. The current density is not uniform on the surface; it is a function of the shape and separation of the conductors.[3] With time, the current and associated magnetic field diffuse into the conductors.[4] Because large current densities are involved, local heating occurs in the rails. This changes rail properties such as the electrical conductivity. Thus, the current-diffusion process is nonlinear in rail-gun conductors. In addition, thermal diffusion is occurring simultaneously with current diffusion. The thermal-diffusion process is also nonlinear. The time scale over which current diffusion occurs is so short (milliseconds) that thermal diffusion is normally neglected.[4]

Most analyses of these phenomena have dealt with magnetic-field diffusion in flux-compression generators.[4-6] The results of Kidder are particularly appropriate as an example of nonlinear diffusion of a magnetic field in one dimension.[7] Analysis of rail-gun conductors presents a more difficult and somewhat different problem because the rails require a two-dimensional calculation and because current and not magnetic field is the primary variable. In the linear case, magnetic field strength and current density obey the same partial differential equation, the linear thermal-diffusion equation.[4] This is no longer true in the nonlinear case. In a two-dimensional, nonlinear calculation, coupled partial-differential equations for the components of a vector quantity such as the magnetic-field strength may be required. Thus, the geometry of a problem and the quantities known as initial and boundary conditions play a very important part in the complexity of the solution.

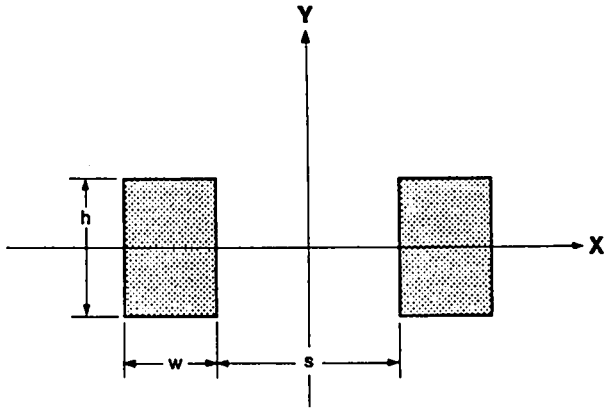

Fig. 2. Cross section of two rectangular rails.

This report describes a formulation of the current-diffusion problem that is appropriate to two-dimensional, nonlinear calculations for rail-gun conductors. This formulation has been applied by adapting a finite-difference, heat-transfer computer program to the calculation of current diffusion. The calculation can include or neglect thermal diffusion, so as to test its influence on the resulting temperatures. This calculation method has been applied to a series of different-size rectangular rails. Results for current density and temperature as a function of time and location in the rail are presented. Some general conclusions drawn from these results are discussed. Two test problems, in which one-dimensional results obtained by this calculation method are compared with other analyses, are also presented.

II. CURRENT AND FIELD DIFFUSION

The starting point for the formulation of a current- or field-diffusion problem is three of Maxwell's equations[4]

$$\nabla \times \overline{H} = \overline{J} \quad , \tag{1}$$

$$\nabla \times \overline{E} = - \partial \overline{B} / \partial t = - \mu \partial \overline{H} / \partial t \quad , \tag{2}$$

and

$$\overline{J} = \sigma \overline{E} \quad . \tag{3}$$

In these equations, $\overline{H}$ is magnetic-field intensity, $\overline{B}$ is the magnetic induction, $\overline{E}$ is electric-field intensity, and $\overline{J}$ is current density; all are vector quantities. In addition, t is time, σ is electrical conductivity, and μ is magnetic permeability. Two restrictions inherent in these equations as written are that displacement currents have been neglected in Eq. (1) and μ has been assumed constant in Eq. (2). The neglect of displacement currents is normal for these calculations.[4] The second restriction means that this formulation does not apply to ferromagnetic materials. The assumption of constant μ is removed in a later development in this section.

Most analyses of these phenomena have dealt with magnetic-field diffusion in flux-compression generators.[4-6] This formulation will be developed first; later it will be compared with a formulation in terms of current diffusion. Taking the curl of Eq. (1) gives

$$\nabla X \nabla X \overline{H} = \nabla(\nabla \cdot \overline{H}) - \nabla^2 \overline{H} = \nabla X \overline{J} \quad , \tag{4}$$

where a vector identity for $\nabla X \nabla X \overline{H}$ has been employed.[4] As long as μ is constant, $\nabla \cdot \overline{H} = 0$, giving $\nabla(\nabla \cdot H) = 0$ in Eq. (4). Using Eq. (3) and then Eq. (2), Eq. (4) can be written as

$$-\nabla^2 \overline{H} = \nabla X(\sigma \overline{E}) = \nabla \sigma X \overline{E} + \sigma(\nabla X \overline{E}) \quad ,$$

or

$$-\nabla^2 \overline{H} = -\mu\sigma(\partial \overline{H}/\partial t) + \nabla \sigma X \overline{E} \quad . \tag{5}$$

The quantity $\overline{E}$ can be eliminated from Eq. (5) by employing Eqs. (3) and (1),

$$\begin{aligned} -\nabla^2 \overline{H} + \mu\sigma(\partial \overline{H}/\partial t) &= \nabla \sigma X(\overline{J}/\sigma) \\ &= \nabla \sigma X[(1/\sigma)(\nabla X \overline{H})] \\ &= (1/\sigma)[\nabla \sigma X(\nabla X \overline{H})] \quad . \end{aligned} \tag{6}$$

If σ is not a function of temperature or position, $\nabla \sigma = 0$, and Eq. (6) reduces to the linear thermal-diffusion equation[8]

$$\nabla^2 \overline{H} = \mu\sigma(\partial \overline{H}/\partial t) \quad , \tag{7}$$

where $(\mu\sigma)^{-1}$ is analogous to the thermal diffusivity. The magnetic-field intensity ($\overline{H}$) is a vector quantity; in a cartesian coordinate system, Eq. (7) implies three equations in the three components of $\overline{H}$,

$$\nabla^2 H_x = \mu\sigma(\partial H_x/\partial t) \quad , \tag{8a}$$

$$\nabla^2 H_y = \mu\sigma(\partial H_y/\partial t) \quad , \tag{8b}$$

and

$$\nabla^2 H_z = \mu\sigma(\partial H_z/\partial t) \quad . \tag{8c}$$

These equations are not coupled because each equation contains only one of the components of $\overline{H}$. If σ is a function of position (x,y,z), then

$$\nabla \sigma = (\partial\sigma/\partial x)e_x + (\partial\sigma/\partial y)e_y + (\partial\sigma/\partial z)e_z \quad ,$$

where e_x, e_y, and e_z are unit vectors in the x, y, and z directions, respectively. If σ is a function of temperature (T), which in turn is a function of position because of local heating,

$$\begin{aligned} \nabla \sigma = (d\sigma/dT)\nabla T = (d\sigma/dT)[&(\partial T/\partial x)e_x \\ &+ (\partial T/\partial y)e_y + (\partial T/\partial z)e_z] \quad . \end{aligned}$$

In either case, Eq. (6) is very complicated for the general three-dimensional problem. The three cartesian components of H can be written as

$$\begin{aligned} \nabla^2 H_x - \mu\sigma(\partial H_x/\partial t) = -(1/\sigma)\{&(\partial\sigma/\partial y)[(\partial H_y/\partial x) \\ &- (\partial H_x/\partial y)] - (\partial\sigma/\partial z)[(\partial H_x/\partial z) \\ &- (\partial H_z/\partial x)]\} \quad , \end{aligned} \tag{9a}$$

$$\begin{aligned} \nabla^2 H_y - \mu\sigma(\partial H_y/\partial t) = -(1/\sigma)\{&(\partial\sigma/\partial z)[(\partial H_z/\partial y) \\ &- (\partial H_y/\partial z)] - (\partial\sigma/\partial x)[(\partial H_y/\partial x) \\ &- (\partial H_x/\partial y)]\} \quad , \end{aligned} \tag{9b}$$

and

$$\begin{aligned} \nabla^2 H_z - \mu\sigma(\partial H_z/\partial t) = -(1/\sigma)\{&(\partial\sigma/\partial x)[(\partial H_x/\partial z) \\ &- (\partial H_z/\partial x)] - (\partial\sigma/\partial y)[(\partial H_z/\partial y) \\ &- (\partial H_y/\partial z)]\} \quad . \end{aligned} \tag{9c}$$

These three partial-differential equations are coupled as each equation contains the three components of $\overline{H}$. These equations, as well as Eq. (6), can still be considered diffusion equations, where the quantities on the right-hand side of each equation represent source terms.[8]

For certain special problems, Eqs. (9) simplify considerably. In the one-dimensional problem where $H_x = H_y = 0$ and H_z and σ are functions of x only, one equation remains

$$\partial^2 H_z/\partial x^2 - \mu\sigma(\partial H_z/\partial t) = (1/\sigma)(\partial\sigma/\partial x)(\partial H_z/\partial x) \quad . \quad (10)$$

If the electrical resistivity ($\rho = 1/\sigma$) is used in place of σ, Eq. (10) can be rewritten as

$$\frac{\partial}{\partial x}\left(\rho \frac{\partial H_z}{\partial x}\right) = \mu(\partial H_z/\partial t) \quad , \quad (11)$$

which is analogous to the one-dimensional thermal-diffusion equation with variable conductivity.[8] This equation is often used for field-diffusion calculations in flux-compression generators.[4-6] For the rail-gun conductors shown in Fig. 2, $\overline{H}$ will have two components, H_x and H_y, and σ and T will be functions of x and y. Equations (9) will then reduce to

$$\nabla^2 H_x - \mu\sigma(\partial H_x/\partial t) = -(1/\sigma)(\partial\sigma/\partial y)[(\partial H_y/\partial x) - (\partial H_x/\partial y)] \quad , \quad (12a)$$

and

$$\nabla^2 H_y - \mu\sigma(\partial H_y/\partial t) = (1/\sigma)(\partial\sigma/\partial x)[(\partial H_y/\partial x) - (\partial H_x/\partial y)] \quad . \quad (12b)$$

These equations still represent two coupled partial-differential equations that would be difficult to solve.

A diffusion problem can also be formulated in terms of current density or electric-field-strength diffusion. Taking the curl of Eq. (2) gives

$$\nabla\times\nabla\times\overline{E} = \nabla(\nabla\cdot\overline{E}) - \nabla^2\overline{E} = -\mu\left[\frac{\partial}{\partial t}(\nabla\times\overline{H})\right] \quad . \quad (13)$$

If the free charge density is zero, then $\nabla\cdot\overline{E} = 0$; this is a valid assumption for the high current and field problems involving rail guns. Using Eqs. (1) and (3) in Eq. (13) results in

$$\nabla^2(\overline{J}/\sigma) = \mu(\partial\overline{J}/\partial t) \quad , \quad (14)$$

or in terms of $\overline{E}$,

$$\nabla^2\overline{E} = \mu[\partial(\sigma\overline{E})/\partial t] \quad . \quad (15)$$

If σ is not a function of position, time, or temperature, Eqs. (14) and (15) have the same form as Eq. (7); that is, they are the linear thermal-diffusion equation. For a given problem, the boundary conditions and initial conditions for $\overline{H}$, $\overline{J}$, and $\overline{E}$ will be different; thus, although they obey the same differential equation, the solutions for these quantities will differ. If σ is a function of temperature, which can vary with time and position, Eq. (15) results in a particularly straightforward formulation

$$\nabla^2\overline{E} = \mu\sigma(\partial\overline{E}/\partial t) + \mu\overline{E}(\partial\sigma/\partial t) \quad . \quad (16)$$

Equations for the three cartesian components of $\overline{E}$ can be easily written from Eq. (16),

$$\nabla^2 E_x = \mu\sigma(\partial E_x/\partial t) + \mu E_x(\partial\sigma/\partial t) \quad , \quad (17a)$$

$$\nabla^2 E_y = \mu\sigma(\partial E_y/\partial t) + \mu E_y(\partial\sigma/\partial t) \quad , \quad (17b)$$

and

$$\nabla^2 E_z = \mu\sigma(\partial E_z/\partial t) + \mu E_z(\partial\sigma/\partial t) \quad . \quad (17c)$$

These equations are not coupled, thereby simplifying the analysis of a multidimensional problem.

Analysis of current diffusion in rail-gun conductors is particularly simple because the current density and electric field strength have only one nonzero cartesian component, the z-component, which is a function of x, y, and t (see Fig. 2). Of Eqs. (17), only Eq. (17c) remains, resulting in

$$(\partial^2 E_z/\partial x^2) + (\partial^2 E_z/\partial y^2) = \mu\sigma(\partial E_z/\partial t) + \mu E_z(\partial\sigma/\partial t) \quad . \quad (18)$$

In the language of thermal diffusion, E_z is equivalent to temperature, $(\mu\sigma)$ is volumetric heat capacity, the thermal conductivity is one, and $[-\mu E_z(\partial\sigma/\partial t)]$ is equivalent to an energy generation or source term per unit volume.[8] Equation (18) was used to calculate current density as a function of time and position in rail-gun conductors. Local values of the current density and electric field strength were related by

$$j_z = \sigma E_z \quad .$$

The development to this point has been based on the assumption that the magnetic permeability, μ, is constant. This assumption can be relaxed at the expense of additional complexity in the resulting equations. Variable permeability is usually written as $\mu = \mu_0\mu_r(H)$, where μ_0 is $4\pi \times 10^{-7}$ H/m and μ_r is the relative permeability, which is written as a function H, the magnitude of the magnetic-field strength $(\overline{H})$. Relative permeability data are tabulated for many materials.[9] Because μ is no longer constant, Eq. (2) becomes

$$\nabla \times \overline{E} = -\mu_0 \partial(\mu_r \overline{H})/\partial t \quad . \tag{19}$$

This change would affect all of the previous derivations. However, only the current-diffusion formulation will be discussed here. The development parallels that for Eqs. (13) to (18), except that Eq. (19) is used in place of Eq. (2) and that the dependence of μ_r on H, and thus on position and time, is recognized. The equivalent of Eq. (15) is

$$\nabla^2 \overline{E} = \mu_0[\partial(\mu_r \sigma \overline{E})/\partial t] + \mu_0[\partial(\nabla \mu_r \times \overline{H})/\partial t] \quad . \tag{20}$$

In addition to the variation of μ_r with time that is included in the first term on the right-hand side of Eq. (20), an additional term involving the magnetic field has been introduced. For the two-dimensional rail-gun problem, the equivalent to Eq. (18) is

$$(\partial^2 E_z/\partial x^2) + (\partial^2 E_z/\partial y^2) = \mu_0\mu_r\sigma(\partial E_z/\partial t) + \mu_0 E_z[\partial(\mu_r\sigma)/\partial t] + \mu_0\partial\{\mu_r'[(\partial H/\partial x)H_y - (\partial H/\partial y)H_x]\}/\partial t \quad , \tag{21}$$

where $\mu_r' = d\mu_r/dH$. The second and third terms on the right-hand side of Eq. (21) are analogous to the source terms of a diffusion problem. These terms are considerably more complex than in the formulation for constant μ because the magnetic field must now be known. For a one-dimensional problem in which E_z, j_z, and H_x are the only nonzero components and are functions of y and t,

$$(\partial^2 E_z/\partial y^2) = \mu_0\mu_r\sigma(\partial E_z/\partial t) + \mu_0 E_z[\partial(\mu_r\sigma)/\partial t] - \mu_0\partial[\mu_r'H(\partial H/\partial y)]/\partial t \quad , \tag{22}$$

where $H_x = H$ in this case. Equation (22) can be rearranged with the aid of the relation

$$j_z = \sigma E_z = -\partial H/\partial y \quad , \tag{23}$$

for this one-dimensional case. This gives

$$(\partial^2 E_z/\partial y^2) = \mu_0\sigma(\mu_r + H\mu_r')(\partial E_z/\partial t) + \mu_0 E_z\partial[\sigma(\mu_r + H\mu_r')]/\partial t \quad . \tag{24}$$

Equation (24) is analogous to a thermal-diffusion equation where E_z is the temperature, $\mu_0\sigma(\mu_r + H\mu_r')$ is the volumetric heat capacity, the thermal conductivity is one, and $-\mu_0 E_z\partial[\sigma(\mu_r + H\mu_r')]/\partial t$ is a source term per unit volume.[8]

Formulations of the current-diffusion problem for nonferromagnetic material (μ constant) and ferromagnetic material (μ is a function of the magnitude of the magnetic strength) have been developed. Although the solution with variable μ is a more general development, it has not been pursued for rail-gun conductors because they are generally made of copper or other nonferromagnetic materials. A comparison of one-dimensional current diffusion for ferromagnetic and nonferromagnetic materials is given as an example of the use of Eq. (24).

III. FINITE-DIFFERENCE FORMULATION

Even though Eq. (18) represents a relatively simple approach to the solution of current- and field-diffusion problems in rail-gun conductors, it is much too complex for an analytic solution.

Because of the similarity of this problem to thermal-diffusion calculations, a finite-difference, heat-transfer computer program was adapted to solve Eq. (18). The CINDA program was used.[10] Any heat-transfer program of sufficient generality could be employed, however. This section describes the finite-difference formulation of the problem.

The geometry of the conductors shown in Fig. 2 is symmetric about the x and y axes. Thus, it was necessary to model only one half of one conductor, the portion in the first quadrant. No current or thermal diffusion was allowed across the x axis. A 10 by 10 rectangular mesh was used (see Fig. 3). A relatively coarse mesh was employed at this early stage of the work to minimize the use of computer time; a finer mesh will be used in the future if it is warranted. The mesh spacing was variable so that edge and corner nodes, where thermal and current-density gradients were steep, could be made smaller. For the calculations discussed later, the relative node spacing in the x direction (from left to right in Fig. 3) was 0.1, 0.3, 0.6, 1.0, 1.0, 1.0, 1.0, 1.0, 0.5, and 0.1, and the relative node spacing in the y direction (from top to bottom) was 0.2, 0.5, 1.0, 1.0, 1.0, 1.0, 1.0, 1.0, 1.0, and 1.0.

For these calculations, it was assumed that the total current in the conductor was known as a function of time. Changes in total current were made by changing the current density in the edge nodes only; that is, it was assumed that current density or electric field strength enters or leaves the conductor through its exterior surface. The surface current-density distribution (in units of current per unit length) was obtained from static calculations of the high-frequency inductance of the conductors.[3] This distribution varies with the size and separation of the conductors. It was converted into a current density in the edge nodes (in units of current per unit area) by distributing all the current on the surface of a given edge node uniformly over the node area. With this procedure, each edge node requires a source term (which can be positive or negative, depending on how the total current is changing with time) of the form

$$S_k = \mu A_k \Delta j_k / \Delta t \quad ,$$

where Δj_k is the change in current density of edge node k required over time step Δt, and A_k is the area of edge node k. To determine Δj_k, let j_k' be the relative current density in edge node k based on the surface distribution noted above. The j_k' are normalized so that

$$\sum_{k=1}^{Ne} A_k \, j_k' = 1 \quad , \tag{25}$$

where Ne is the number of edge nodes. Then,

$$\Delta j_k = j_k'(I^n - I^{n-1}) \quad ,$$

where I^n and I^{n-1} are the total currents at times t^n and t^{n-1}, and $\Delta t = t^n - t^{n-1}$. This method distributes the change in total current for a particular time step (t^{n-1} to t^n) among the edge nodes in proportion to their static surface current distribution in the high-frequency limit. The source term for edge node k becomes

$$S_k^n = \mu A_k j_k'(I^n - I^{n-1})/\Delta t \quad , \tag{26}$$

and the total source for the entire mesh is

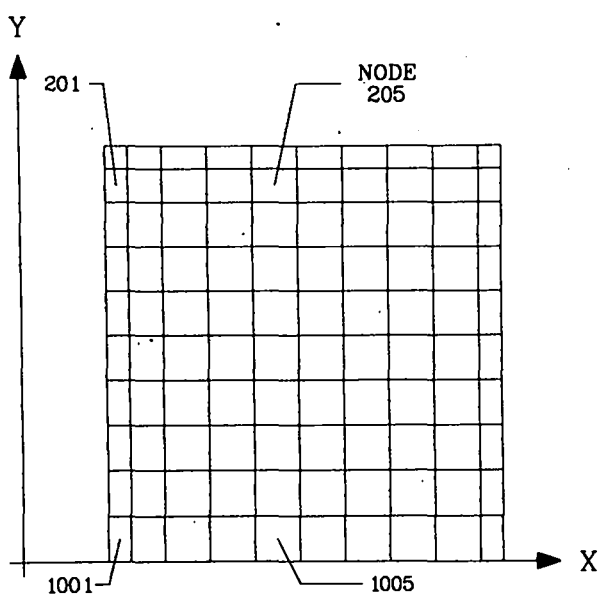

Fig. 3. A 10 by 10 rectangular mesh on half of one rail.

$$S_T^n = \sum_{k=1}^{Ne} S_k^n = \mu(I^n - I^{n-1})/\Delta t \quad ,$$

where Eq. (25) was used.

In addition to source terms related to changes in the total current, which occur only in edge nodes, Eq. (18) indicates that each node has a source term that is related to the change in conductivity of the node with time. For node i in the mesh, a source term of the form

$$S_i^{n+1} = -\mu A_i j_i^n \, (\sigma_i^n - \sigma_i^{n-1})/(\sigma_i^n \, \Delta t) \qquad (27)$$

is used, where A_i is the area of node i, and j_i^n and σ_i^n are the current density and conductivity of node i at time step n. The derivative $(\partial\sigma/\partial t)$ in Eq. (18) has been approximated by the change in conductivity over one time step, and E_z for node i is written as (j_i/σ_i).

To follow the conductivity of each node with time, the node temperatures must be known. Node temperatures change during the calculation from resistive heating of the conductor. For node i at time t^n, the energy generation (in W/m^3) was calculated as $(j_i^n)^2/\sigma_i^n$. Two temperature calculations have been performed in this analysis. The simplest gives an adiabatic temperature of each node; it is assumed that all the energy generated in a given node goes into raising that node's temperature. Conduction among the nodes is ignored for the adiabatic-temperature calculation. The adiabatic temperature is only an approximation to the true temperature distribution in the conductor, however. In reality, thermal diffusion is occurring simultaneously with current diffusion. A diffusion temperature for which transient thermal diffusion is considered has also been calculated. For this analysis, a thermal mesh, with the same geometry as the current-density mesh, is set up and the energy generation in each node is used as an energy source term in the thermal-diffusion calculation.[8] Values of the current density, conductivity, and temperature from the past time are employed during the current time step. In addition, a surface heat-transfer coefficient is included to account for heat losses from the conductor during the calculation of the diffusion temperature. A value of 100 $W/m^2 \cdot K$ has been used.

Two electrical parameters of the rail-gun conductors can also be calculated as a function of time from the finite-difference formulation of this problem. They are the inductance per unit length (L') and resistance per unit length (R') of the rails. These parameters change as the current-density distribution changes. The inductance is calculated in the same manner as in the high-frequency limit,

$$I \, L' = \mu \int_{-x_1}^{x_1} H_y(x,o)dx \quad , \qquad (28)$$

where I is the total current and $H_y(x,o)$ is the y component of the magnetic-field strength evaluated along the x-axis.[3] In the high-frequency limit, $x_1 = s/2$ because there is no penetration of current into the conductor (see Fig. 2). As current penetrates into the conductor, x_1 becomes greater than s/2. The value of x_1 is estimated as the location within the conductor at which $H_y(x,o)$ changes sign. The magnetic field outside the conductors is calculated as the sum of the fields from each node, considered as an infinite current filament in the z-direction.[3] This allows $H_y(x,o)$ to be evaluated over the range $0 \leq x \leq s/2$. Inside the conductor, the relation

$$(\partial H_y/\partial x) = -j_z$$

is integrated along the x-axis for $x \geq s/2$.[4] Equation (28) is evaluated using 10-point Gauss quadrature.[11]

The resistance is calculated from the total energy generation in the conductor at a given time. The total current flow is

$$I = \sum_{i=1}^{N} j_i \, A_i \quad ,$$

and the total energy generation is

$$Q = \sum_{i=1}^{N} j_i^2 A_i/\sigma_i \quad ,$$

where N is the total number of nodes in the mesh. Thus, the resistance per unit length can be written as

$$R' I^2 = Q = \sum_{i=1}^{N} j_i^2 A_i/\sigma_i \quad . \tag{29}$$

Values of R' obtained near the start of a calculation will be inaccurate because they depend on the size of the edge nodes in the mesh. After diffusion has carried the current into the nodes adjacent to the edge nodes and beyond, R' should accurately represent the average resistance of the conductor.

Two one-dimensional test problems and a one-dimensional calculation involving ferromagnetic material were also done. A one-dimensional mesh of 50 nodes with uniform node spacing was used for these calculations. In other respects, the two test problems were the same as the two-dimensional formulation just described. For the one-dimensional ferromagnetic calculation, Eq. (24) was used as the basis for the finite-difference calculation. The magnetic field (H) was calculated by integrating Eq. (23) through the conductor. At the surface y = 0

$$H(y=0) = \sum_{i=1}^{N} j_i \, \Delta y_i \quad ,$$

where j_i is the current density and Δy_i is the node spacing of node i, and N is the total number of nodes. The quantity $(\mu_r + H\mu_r')$ in Eq. (24) was expressed as a function of H. Some numerical problems were encountered during the ferromagnetic calculation because $(\mu_r + H\mu_r')$ varies over a range of $\sim 10^4$ as H changes from zero to the saturation field for the conductor.[9] Because the saturation field of most ferromagnetic materials is quite small compared to the magnetic fields encountered in rail-gun conductors, this change occurred over a few normal time steps. These problems were generally eliminated by reducing the time step by a factor of 100 to 1000 whenever any node was passing through the saturation field. Occasional small perturbations were still seen in the current density of a node at this time; however, these perturbations damped out quickly.

IV. ONE-DIMENSIONAL TEST PROBLEMS

Two one-dimensional test problems were run to compare the results of the current-diffusion formulation with other analyses. The first test problem was a comparison with the magnetic field-diffusion calculations of Kidder.[7] He calculated field diffusion into a semi-infinite half plane resulting from a step change in the magnetic-field strength at the surface. The conductivity of the material was assumed to be inversely proportional to the absolute temperature, so that this is a nonlinear problem. Kidder also calculated the current density that resulted from the magnetic field. The current-diffusion formulation described here was used to calculate current diffusion directly; the initial condition was a step change in total current, which is equivalent to the initial condition on the magnetic field. Because the mesh used here had a finite thickness compared to the semi-infinite half plane in Kidder's analysis, comparisons were made early in the calculation when the current density at the back of the mesh was still near zero. Figure 4 shows a comparison of the current densities at 0.1 and 0.2 ms into the calculation for a total current of 105.8 MA/m (H_0 = 1.33 MG in Ref. 7). The comparison is quite good.

The second test problem was a calculation of the current-density distribution in a semi-infinite half plane where the total current varies sinusoidally with time. The conductivity was assumed to be constant so this is a linear problem. However, it does test the manner in which current is added and removed at the surface of a conductor. This problem can be solved exactly and is the basis of the calculation of the frequency effect in high-frequency ac conductors.[12] The finite-difference calculation used 50 nodes with a node thickness of 0.20 mm. The total current was assumed to vary as

$$I(t) = I_m \sin(2\pi ft) \quad , \tag{30}$$

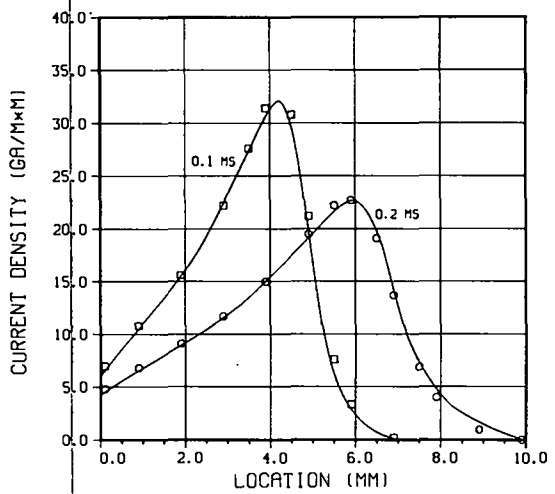

Fig. 4. Comparison of current densities in a semi-infinite half plane at 0.1 ms and 0.2 ms; lines from Ref. 7 and points from finite-difference solution.

where I_m is the maximum current. A frequency (f) of 2000 Hz was used; at this frequency, current diffusion to the back side of the mesh was negligible for the conductivity assumed [$\sigma = 5.28 \times 10^7$ $(\text{ohm-m})^{-1}$]. The current density in a semi-infinite conductor resulting from a sinusoidal excitation can be written as[12]

$$j_z(x,t) = j_0 \exp(-x/\delta) \sin[2\pi ft - (x/\delta) + \theta] \quad , \quad (31)$$

where $\delta = (\mu\sigma\pi f)^{-1/2}$, θ is an arbitrary phase angle, and x is location in the conductor measured from the surface of the conductor. The surface current density is

$$j_z(0,t) = j_0 \sin(2\pi ft + \theta) \quad , \quad (32)$$

where j_0 can be recognized as the peak surface current density. The total current in the conductor is

$$I(t) = \int_0^\infty j_z(x,t)dx$$

$$= (j_0\delta/\sqrt{2}) \sin[2\pi ft - (\pi/4) + \theta] \quad . \quad (33)$$

Comparing Eqs. (32) and (33), the total current and surface current density are seen to be 45° ($\pi/4$ radians) out of phase. If θ is taken as $\pi/4$, Eqs. (33) and (30) are the same, and

$$I_m = j_0\delta/\sqrt{2} \quad .$$

Current densities obtained from the finite-difference current-diffusion calculation are compared with results from Eq. (31) in Figs. 5 and 6, where the solid lines represent the analytic result and the points represent current densities at some of the finite-difference nodes. The finite-difference calculations were run for five cycles; steady-state behavior had been achieved by this time. Figure 5 is at the start of a cycle, where I = 0 A/m. Figure 6 is 4.375×10^{-4} s later (7/8 of the way through a cycle); at this time, I = -70.7 A/m and the surface current density is zero. The agreement is excellent in both cases.

V. CURRENT-DIFFUSION CALCULATIONS FOR RECTANGULAR RAILS

A series of calculations of current diffusion in rectangular rails has been done. The objective of these calculations was to compare rail temperatures for a series of different-size rails that would produce the same acceleration for a projectile of a given mass. The rail separation was assumed to be fixed at 10 mm and the force required was taken as 1×10^5 N. The force was related

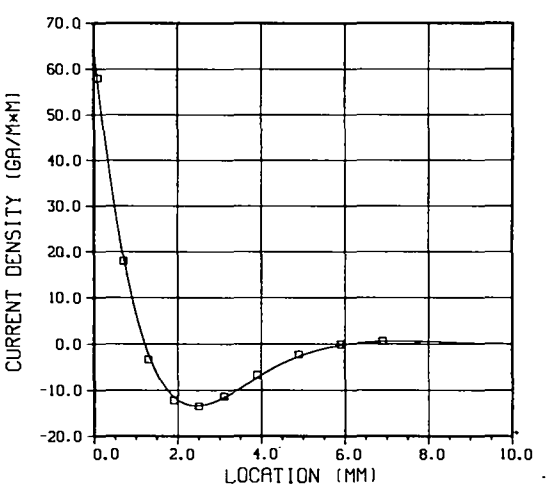

Fig. 5. Comparison of current density in a semi-infinite half plane with a sinusoidal variation of total current; total current = 0 A/m; line is analytic solution and points are finite-difference solution.

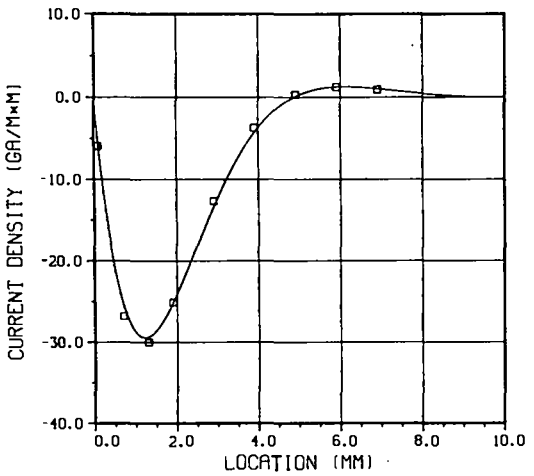

Fig. 6. Comparison of current density in a semi-infinite half plane with a sinusoidal variation of total current; total current = -70.7 A/m; line is analytic solution and points are finite-difference solution.

to the total current (I) and the rail inductance per unit length (L') as[13]

$$F = 1/2\ L'\ I^2 \quad .$$

Thus, if L' is known, I can be calculated as

$$I = [2 \times 10^5/L']^{1/2} \quad .$$

The total current was assumed constant during the diffusion calculation. The value of L' used to calculate I was taken as the inductance in the high-frequency limit,[3] even though L' changes as current diffusion occurs. Table I shows calculated values of L', I, and the ratio of I to the conductor area (A) and perimeter (P). Even before diffusion calculations are done, some general comments can be made about the relative merits of various rail sizes. Figures 7 and 8 show plots of I/A and I/P as a function of rail width (w) for the data from Table I. Even though the current is not distributed uniformly over the rail surface or the cross-sectional area, these parameters provide some measure of heating. For a given rail height (h), I decreases as the rail width (w) is made smaller (see Table I); however, both I/A and I/P increase as w decreases. This would indicate that the rail size should be as large as practical to minimize

TABLE I

RAIL PARAMETERS

h[a] (mm)	w[a] (mm)	L' (μH/m)	I (MA)	I/A (MA/m^2)	I/P (MA/m)
2	5	0.790	0.503	50.3 x 10^3	35.9
	2	0.921	0.466	116.5 x 10^3	58.3
	1	1.007	0.446	223.0 x 10^3	74.3
5	10[b]	0.575	0.590	11.8 x 10^3	19.7
	5	0.640	0.559	22.4 x 10^3	28.0
	2	0.715	0.529	52.9 x 10^3	37.8
	1	0.758	0.514	102.8 x 10^3	42.8
10	20	0.413	0.696	3.5 x 10^3	11.6
	15	0.431	0.681	4.5 x 10^3	13.6
	10[b]	0.456	0.662	6.6 x 10^3	16.6
	5[b]	0.495	0.636	12.7 x 10^3	21.2
	2	0.536	0.611	30.6 x 10^3	25.5
	1	0.556	0.600	60.0 x 10^3	27.3
15	15	0.362	0.743	3.3 x 10^3	12.4
	10[b]	0.380	0.725	4.8 x 10^3	14.5
	5[b]	0.407	0.701	9.4 x 10^3	17.5
20	20	0.303	0.812	2.0 x 10^3	10.2
	15	0.313	0.799	2.7 x 10^3	11.4
	10	0.327	0.782	3.9 x 10^3	13.0
	5[b]	0.347	0.759	7.6 x 10^3	15.2

[a] h = rail height and w = rail width; see Fig. 2.

[b] Current diffusion calculation performed.

rail heating. For a given rail area, rails with larger width have a larger value of L' and thus, a lower value of I. For example, a h = 10 mm by w = 15 mm rail requires I = 0.681 MA, but a h = 15 mm by w = 10 mm rail requires I = 0.725 MA

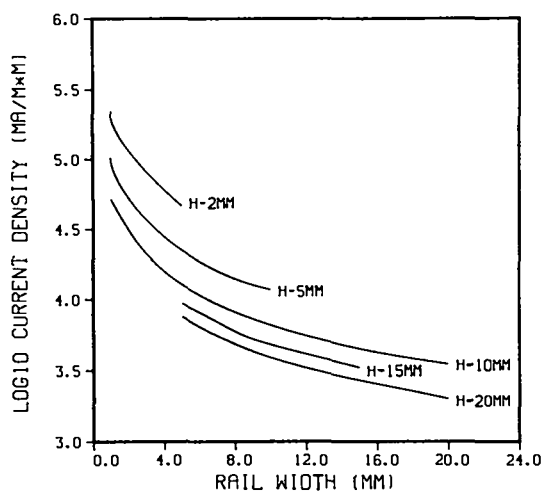

Fig. 7. Plot of current density I/A as a function of rail width.

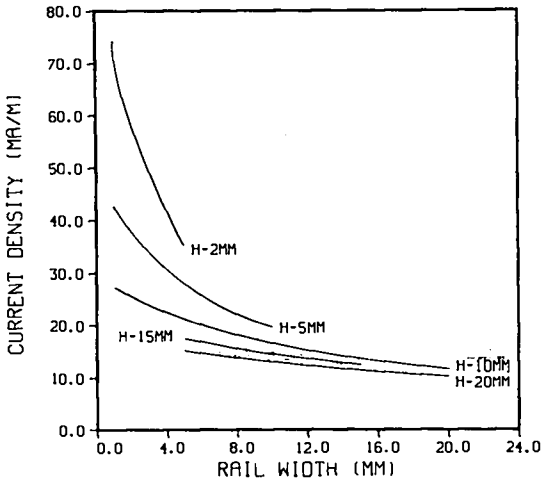

Fig. 8. Plot of surface current density I/P as a function of rail width.

to achieve the same force. Thus, the wider rail would show less heating.

The surface current distributions for the various size rails were calculated at the same time as the inductance.[3] For the calculations of these quantities, the rails were assumed to have a corner radius of 0.02 mm, that is, a relatively sharp corner. Figure 9 shows a plot of the relative current density on the rail surface (continuous curve) compared with the average current densities used for the edge nodes (stepped curve) for one rail size (h = 10 mm by w = 10 mm). It is evident that the peaks at the corners of the rails

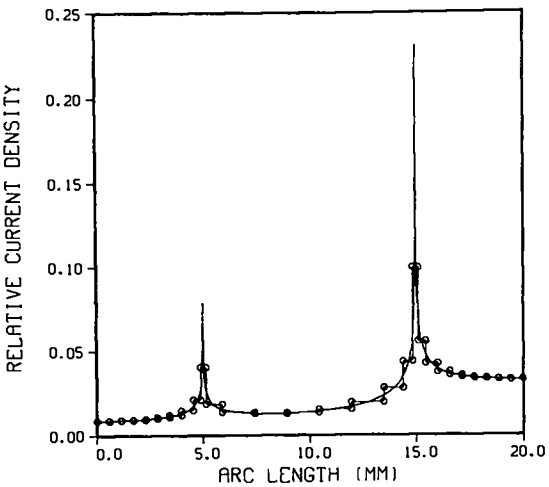

Fig. 9. Current density around surface of 10-mm by 10-mm rail; continuous curve from Ref. 3 and stepped curve is finite-difference approximation.

are not approximated well. A much smaller node size would be required for a better approximation. For this reason, temperatures calculated at the rail corners may not be accurate. The need for a finer mesh size is recognized, but this refinement will be postponed until some verification of the calculated temperatures has been made.

Diffusion calculations were run to 5×10^{-4} s; total current was assumed to rise from zero to the constant values shown in Table I in 1×10^{-8} s with the shape of a quarter sine wave. This would result in a final velocity of 16.7 km/s for a 3-g projectile. The rails were assumed to be copper; the electrical conductivity, volumetric specific heat, and thermal conductivity were defined as a function of temperature.[14] No attempt was made to account for the effects of melting on the properties or on heat transfer. Unless otherwise noted, all of the temperatures reported are adiabatic temperatures; a comparison of adiabatic temperatures and diffusion temperatures for one run is made later.

Diffusion calculations were made for only six of the rail sizes (see Table I). Figure 10 shows a plot of average rail temperature (area average) as a function of time for these rails. The initial temperature was 300 K in all cases. It is evident that the smaller rails (h = 10 mm by w = 5 mm and h = 5 mm by w = 10 mm) would be impractical for these conditions because average rail temperatures in the vicinity of the melting point of copper

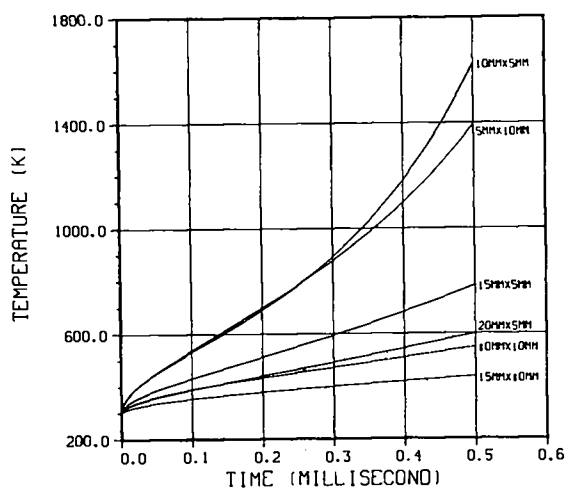

Fig. 10. Average rail temperatures as a function of time.

(1356 K) are attained. Gross melting could be expected of these and smaller rails. Average rail temperatures for the four larger rails are well below the melting point of copper; however, as will be seen later, local melting may occur in these rails.

Local values of the current density and rail temperature cannot be presented in detail for all the cases studied because of the volume of data involved. For this reason, only a sampling of the local data is given. As a start, Table II lists node temperatures for four nodes at two times during the calculation, 1×10^{-4} s and 5×10^{-4} s. The locations of the four nodes are shown in Fig. 3. Node 201, an edge node near the inside corner, is generally one of the highest temperature nodes. Near the vertical center of the conductor on the inside surface (node 1001), temperatures are usually well below those near the inside corner. The two interior nodes (nodes 205 and 1005) show lower temperatures still; node 205, which is near the top edge, has higher temperatures than node 1005, which is near the middle of the conductor. The relative values of the temperatures for all nodes are generally related to their surface current density if they are edge nodes and to their proximity to the surface if they are interior nodes. The two smaller rails (h = 5 mm by w = 10 mm and h = 10 mm by w = 5 mm) show relatively uniform heating at 5×10^{-4} s (see Table II). By this time, current distribution is relatively uniform over the cross section of these small rails, resulting in uniform heating. The same phenomenon is responsible for the upturn in the average rail temperature for these cases that starts between 2×10^{-4} and 3×10^{-4} s (see Fig. 10).

The data for the four larger rail sizes in Table II indicate that most of the temperature rise of the edge nodes (201 and 1001) occurs by 1×10^{-4} s. Figure 11 shows this behavior; the temperature of node 201 for the rails with h = 10 mm by w = 10 mm is plotted as a function of time. This situation is directly related to the current-density behavior; Fig. 12 shows a plot of current density as a function of time for the same node. Time is plotted on a logarithmic scale because most of the current flow occurs in a narrow range of time, early in the calculation. As the conductor is heated, its conductivity drops and current flows more easily in the cooler, inner region of the conductor. This nonlinear behavior accelerates diffusion of the current density.[7] Figures 13 and 14 show plots of temperature and current density as a function of time for node 1005 (an interior node) for the same rails. The time required for the current to diffuse into this node is evident.

The inside surface of the rails, where they contact the projectile, is their most critical

TABLE II
NODE TEMPERATURES FOR VARIOUS RAIL SIZES

Rail Size h (mm)	Rail Size w (mm)	Temperature (K)[a] $t = 1 \times 10^{-4}$ s 201[b]	205	1001	1005	$t = 5 \times 10^{-4}$ s 201	205	1001	1005
5	10	3907	430	1238	327	4179	1470	1959	1457
10	10	2323	373	690	300	2387	596	896	477
10	5	2531	774	771	332	2888	1665	1669	1574
15	10	1648	349	614	300	1710	509	695	345
15	5	1778	648	677	316	1923	1045	828	574
20	5	1405	566	627	313	1533	895	693	414

[a] Initial temperature = 300 K.
[b] Node number (see Fig. 3).

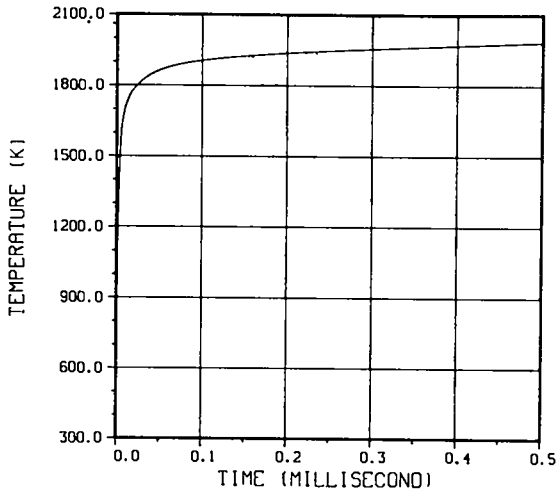

Fig. 11. Node 201 temperature as a function of time for 10-mm by 10-mm rail; see Fig. 3 for node location.

region. Figures 15 and 16 show plots of the inside surface temperature of five of the rails listed in Table II, at 1 x 10^{-4} s. The temperature profile generally follows the surface current-density profile (see Fig. 9). Temperatures along this surface are highest at the corner of the rail. These figures indicate one method of increasing the possibility of reusing rails; if the height of the rails is greater than the height of the projectile, the projectile will not contact the rail corners.where temperatures are highest and rail damage is most likely. This argument ignores problems of arc damage to the rails. Figure 17

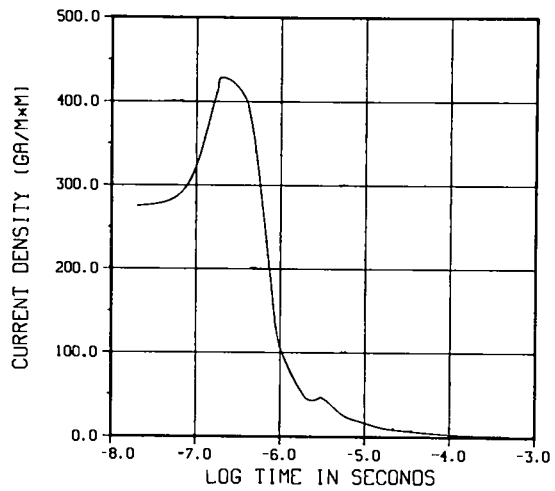

Fig. 12. Node 201 current density as a function of time for 10-mm by 10-mm rail; time plotted as $\log_{10}$ time in seconds; see Fig. 3 for node location.

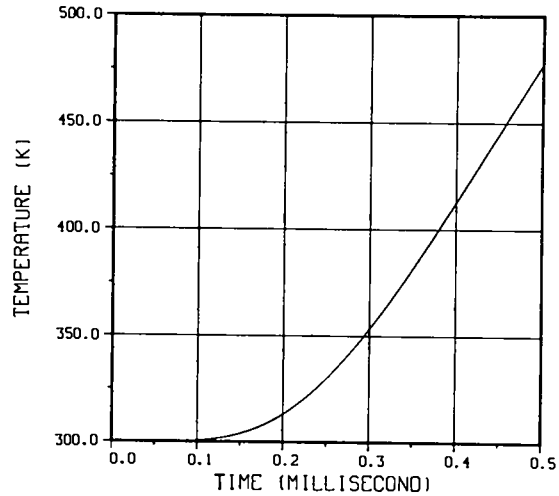

Fig. 13. Node 1005 temperature as a function of time for 10-mm by 10-mm rail; see Fig. 3 for node location.

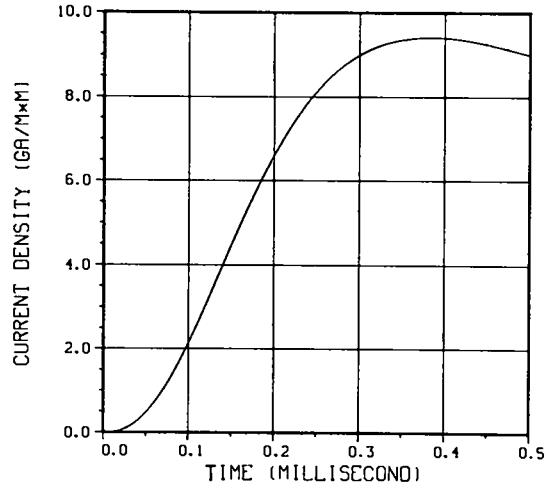

Fig. 14. Node 1005 current density as a function of time for 10-mm by 10-mm rail; see Fig. 3 for node location.

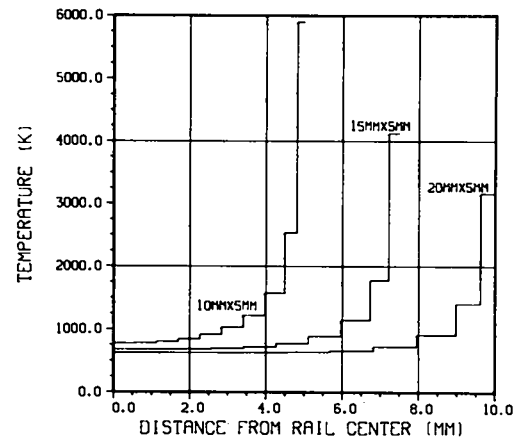

Fig. 15. Inside surface temperature of rails at 0.1 ms.

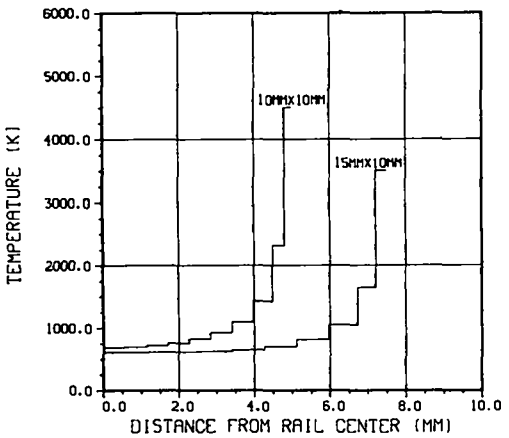

Fig. 16. Inside surface temperature of rails at 0.1 ms.

shows three rail and projectile configurations. In Figs. 17a and 17b, the projectile contacts the corners of the rail, but in Fig. 17c the projectile only contacts the central, cooler section of the rail. Thus, if a 10-mm-high projectile were used in these rails, rail temperatures in the region where the projectile contacts the rail could be limited to ~800 K for h = 15 mm and h = 20 mm rails; rail-surface temperatures above the melting point of copper would occur near the corners where the rail contacts the projectile for h = 10 mm rails.

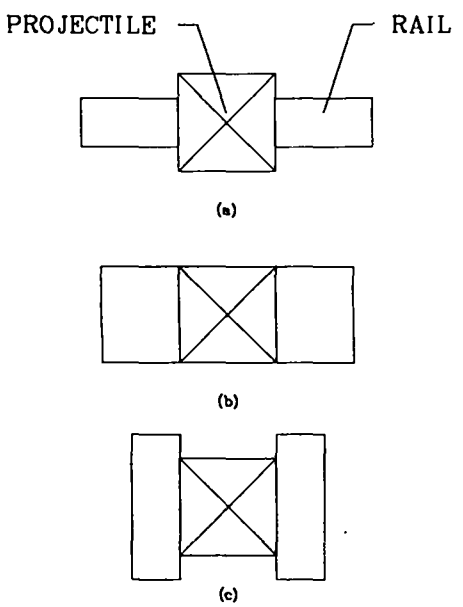

Fig. 17. Three rail and projectile configurations.

The effect of the current rise time, which was 1×10^{-8} s in the previous calculations, was assessed by one calculation for the h = 10 mm by w = 10 mm rail in which the rise time was increased to 1×10^{-5} s. Table III shows a comparison of temperatures of four nodes at two times (0.1 and 0.5 ms) for the two calculations. The most dramatic change is for nodes near the corners, that is, the highest temperature nodes (see node 201 results in Table III). The longer rise time allows time for current to diffuse away from the surface during the initial rise to a constant current. Thus, peak currents and maximum temperatures are lower with a longer rise time.

All of the preceding temperatures have been adiabatic temperatures. A coupled current-diffusion and thermal-diffusion calculation was done for one case, h = 10 mm by w = 10 mm rails. Table IV shows a comparison of the two sets of temperatures obtained. The edge-node (201 and 1001) diffusion temperatures are the same or lower than the adiabatic temperatures because these nodes tend to lose heat to the surroundings or adjacent interior nodes. Interior node diffusion temperatures can be higher than adiabatic temperatures if heat is conducted into the interior nodes from nearby edge nodes. Differences between diffusion and adiabatic temperatures are greater at 5×10^{-4} s than at 1×10^{-4} s; differences would continue to increase with time as thermal conduction occurs. The adiabatic-temperature calculation represents a reasonable approximation at this stage of the work.

TABLE III

COMPARISON OF TEMPERATURES FOR FAST AND SLOW CURRENT RISE TIMES[a]

Time (s)	Current Rise Time (s)	Temperature (K)			
		201[b]	205	1001	1005
1×10^{-4}	1×10^{-8}	2323	373	690	300
1×10^{-4}	1×10^{-5}	1722	366	609	300
5×10^{-4}	1×10^{-8}	2387	596	896	477
5×10^{-4}	1×10^{-5}	1810	587	840	470

[a] h = 10 mm x w = 10 mm rails.

[b] Node number (see Fig. 3).

TABLE IV

COMPARISON OF ADIABATIC AND DIFFUSION TEMPERATURES[a]

Time (s)	Temperature Calculation	Temperature (K) 201[b]	205	1001	1005
1×10^{-4}	Adiabatic	2323	373	690	300
1×10^{-4}	Diffusion	2328	377	658	301
5×10^{-4}	Adiabatic	2387	596	896	477
5×10^{-4}	Diffusion	2121	600	834	480

[a] h = 10 mm x w = 10 mm rails.

[b] Node number (see Fig. 3).

Computer execution times were about three times as long for the diffusion-temperature calculation as for the adiabatic-temperature calculation. On a CDC 7600 computer at Los Alamos, the adiabatic-temperature calculation required ~300 CPU seconds and the diffusion-temperature calculation required ~900 CPU seconds.

Two electrical parameters of the rails, the inductance per unit length (L') and the resistance per unit length (R'), are shown in Figs. 18 and 19 for the h = 10 mm by w = 10 mm rails. The inductance rises from its initial value, where all the current is distributed on the conductor surface, as current diffuses into the rails (see Fig. 18). The initial value calculated by the finite-difference approximation (0.466 μH/m) agrees quite well

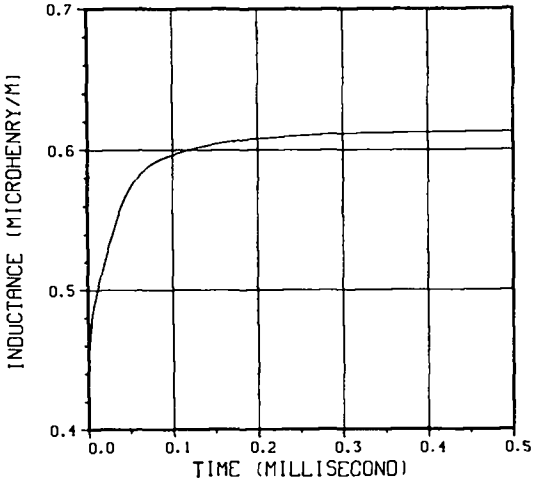

Fig. 18. Inductance of 10-mm by 10-mm rails as a function of time.

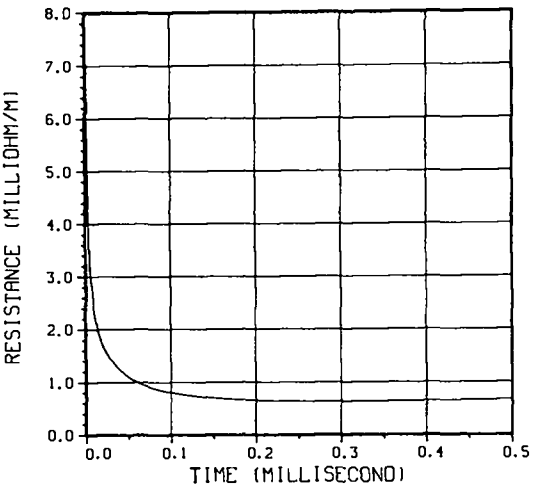

Fig. 19. Resistance of 10-mm by 10-mm rails as a function of time.

with the value calculated by static methods[3] (0.456 μH/m). For a uniform current density, L' calculated by the finite-difference approximation agrees with the result obtained by the method of Grover.[15] Initially, the resistance of the rails is high because current flow is concentrated near the surface of the conductor (see Fig. 19). As the current diffuses into the rails and the current density becomes more uniform, the resistance decreases. Resistance values at early times are probably inaccurate because they depend on the mesh size.

VI. ONE-DIMENSIONAL CURRENT DIFFUSION IN FERROMAGNETIC CONDUCTORS

A one-dimensional calculation was done to assess the influence of ferromagnetism on current diffusion. A 50-node layer with a node thickness of 0.20 mm was used. The initial condition was a step change in total current at one side of the mesh; the resultant current pulse diffused into the conductor. This problem is similar to the test problem that simulated Kidder's results, except that the material was assumed to be iron. The electrical conductivity, thermal conductivity, and specific heat were taken as functions of temperature.[14] The relative permeability was obtained from a review of various analytic functions that can be used to represent magnetization curve data.[9] The magnetization curve is a functional relation between the magnitude of the magnetic

induction (B) and the magnetic-field strength (H); the relative permeability is defined such that

$$B = \mu_0 \mu_r H \quad .$$

The relations used here are

$$B = H/(C_1+C_2H) \text{ for } H \leq H_s \quad , \tag{34a}$$

and

$$B = [H_s/(C_1+C_2H_s)] + \mu_0(H-H_s) \text{ for } H > H_s \quad , \tag{34b}$$

where $C_1 = 88.3$ and $C_2 = 0.620$ when H is in A/m.[9]

Figure 20 shows a plot of current density as a function of location in the conductor for two calculations. The total current for each was 10 MA/m. The solid line, labeled ferromagnetic, represents the current density at 0.05 ms when Eqs. (34) are used to define μ_r. The dashed line, labeled nonferromagnetic, represents the current density at the same time if μ_r is assumed to be one, but all other properties are the same. The current-density pulse is much steeper in the ferromagnetic case because the associated magnetic field at the leading edge of the pulse is less than H_s and the large value of μ_r retards diffusion.

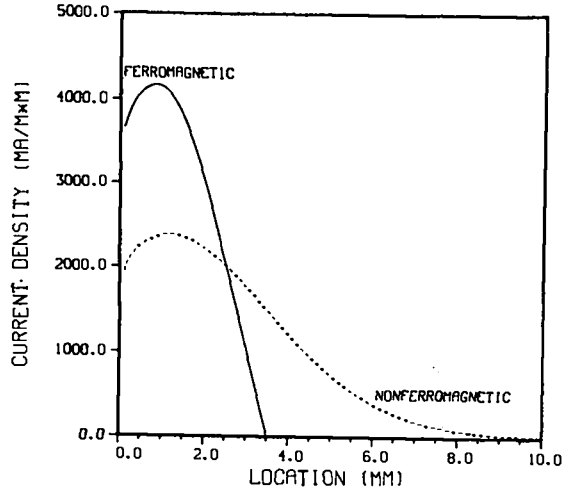

Fig. 20. Comparison of current densities in a semi-infinite half plane at 0.05 ms for a ferromagnetic (solid line) and nonferromagnetic (dashed line) material.

VII. DISCUSSION

The objective of this work was to develop techniques that can be used to assess thermal damage in rail-gun conductors. Joule heating from current flow in the rails is a major source of thermal damage. The nonlinear current-diffusion equation that was developed can be solved in conjunction with the associated thermal-diffusion problem by a finite-difference method. The results of this analysis are rail temperatures as a function of time for a given total current.

The analysis developed here is relatively general. It accounts for the temperature dependence of material properties, in particular, electrical conductivity, which is the major nonlinearity in the current-diffusion calculation for nonferromagnetic materials. The two-dimensional analysis should be capable of accurate temperature calculations if the boundary conditions, initial conditions, and material properties are representative of the actual situation. The material properties of copper, the usual rail material, are relatively well known up to the melting point. The initial conditions are also generally well defined. One of the primary boundary conditions, the initial current distribution on the rail surface, also controls the distribution for adding or removing current as a result of changes in total current flow. This distribution was assumed to be the current distribution on the rail surface in the high-frequency limit (see Fig. 9). The form of this distribution strongly influences the calculated temperature distribution in the rail. The high temperatures at rail corners are caused by the large surface current density there.

This work is part of a continuing study of thermal damage in rail-gun conductors. As part of this study, attempts will be made to experimentally verify calculated rail temperatures. Because rail guns at Los Alamos use a plasma armature, arc damage to the inside rail surfaces also occurs during a test. An attempt will be made to incorporate an arc-damage model into the rail-temperature calculation to more completely model thermal damage in rail-gun conductors.

ACKNOWLEDGMENTS

The author would like to acknowledge the support and encouragement of D. R. Peterson and C. M. Fowler of the Los Alamos National Laboratory in this work.

REFERENCES

1. R. A. Marshall, "The Australian National University Rail Gun Project," Atomic Energy in Australia, 18, 16–18 (1975).

2. S. C. Rashleigh and R. A. Marshall, "Electromagnetic Acceleration of Macroparticles to High Velocities," J. Appl. Phys., 49, 2540–2542 (1978).

3. J. F. Kerrisk, "Current Distribution and Inductance Calculations for Rail-Gun Conductors," Los Alamos National Laboratory report LA-9092-MS (October 1981).

4. H. Knoepfel, Pulsed High Magnetic Fields (North-Holland Publishing Co., Amsterdam, 1970).

5. H. Kolm, B. Lax, F. Bitter, and R. Mills (Eds.), High Magnetic Fields (John Wiley and Sons, Inc., New York, 1962); proc. Int. Conf. on High Magnetic Fields, Cambridge, Massachusetts, November 1–4, 1961.

6. H. Knoepfel and F. Herlach (Eds.), Conf. on Megagauss Magnetic Field Generation by Explosives and Related Experiments [European Atomic Energy Community (Euratom), Brussels, 1966].

7. R. E. Kidder, "Nonlinear Diffusion of Strong Magnetic Fields into a Conducting Half-Space," Lawrence Radiation Laboratory report UCRL-5467 (January 1959).

8. H. S. Carslaw and J. C. Jaeger, Conduction of Heat in Solids (Oxford at the Clarendon Press, London, 1959), Chap. 1.

9. J. Fischer and H. Moser, "Die Nachbildung von Magnetisierungskurnen durch einfache Algebraische oder Transzendente Funktionen," Archin fur Elektrotechnik, 42, 286–299 (1956).

10. R. J. Connor, R. E. Kannady, Jr., and J. E. Almanza, "Adaptation of Chrysler Improved Numerical Differencing Analyzer to CDC 6000 Series Computers," Martin Marietta Corp. report M-68-22 (November 1968).

11. B. Carnahan, H. A. Luther, and J. O. Wilkes, Applied Numerical Methods (John Wiley and Sons, Inc., New York, 1969), Chap. 2.

12. G. Metzger and J. Vabre, Transmission Lines with Pulsed Excitation (Academic Press, New York, 1969), pp. 138–146.

13. S. Seely, Introduction to Electromagnetic Fields (McGraw-Hill Book Co., Inc., New York, 1958), Chap. 9.

14. I. R. McNab, D. W. Deis, V. B. Doshi, D. A. Fikse, H. R. Howland, W. F. Hughes, G. A. Kemeny, P. Reichner, O. S. Taylor, F. J. Young, J. P. Barber, D. Bauer, S. J. Bless, S. Hanchak, and E. Straider, "DC Electromagnetic Launcher Development: Phase I," US Army Armament Research and Development Command report ARLCD-CR-80009 (May 1980).

15. F. W. Grover, Inductance Calculations (D. Van Nostrand Co., Inc., New York, 1946).

Printed in the United States of America
Available from
National Technical Information Service
US Department of Commerce
5285 Port Royal Road
Springfield, VA 22161

Microfiche (A01)

Page Range	NTIS Price Code	Page Range	NTIS Price Code	Page Range	NTIS Price Code	Page Range	NTIS Price Code
001-025	A02	151-175	A08	301-325	A14	451-475	A20
026-050	A03	176-200	A09	326-350	A15	476-500	A21
051-075	A04	201-225	A10	351-375	A16	501-525	A22
076-100	A05	226-250	A11	376-400	A17	526-550	A23
101-125	A06	251-275	A12	401-425	A18	551-575	A24
126-150	A07	276-300	A13	426-450	A19	576-600	A25
						601-up*	A99

*Contact NTIS for a price quote.

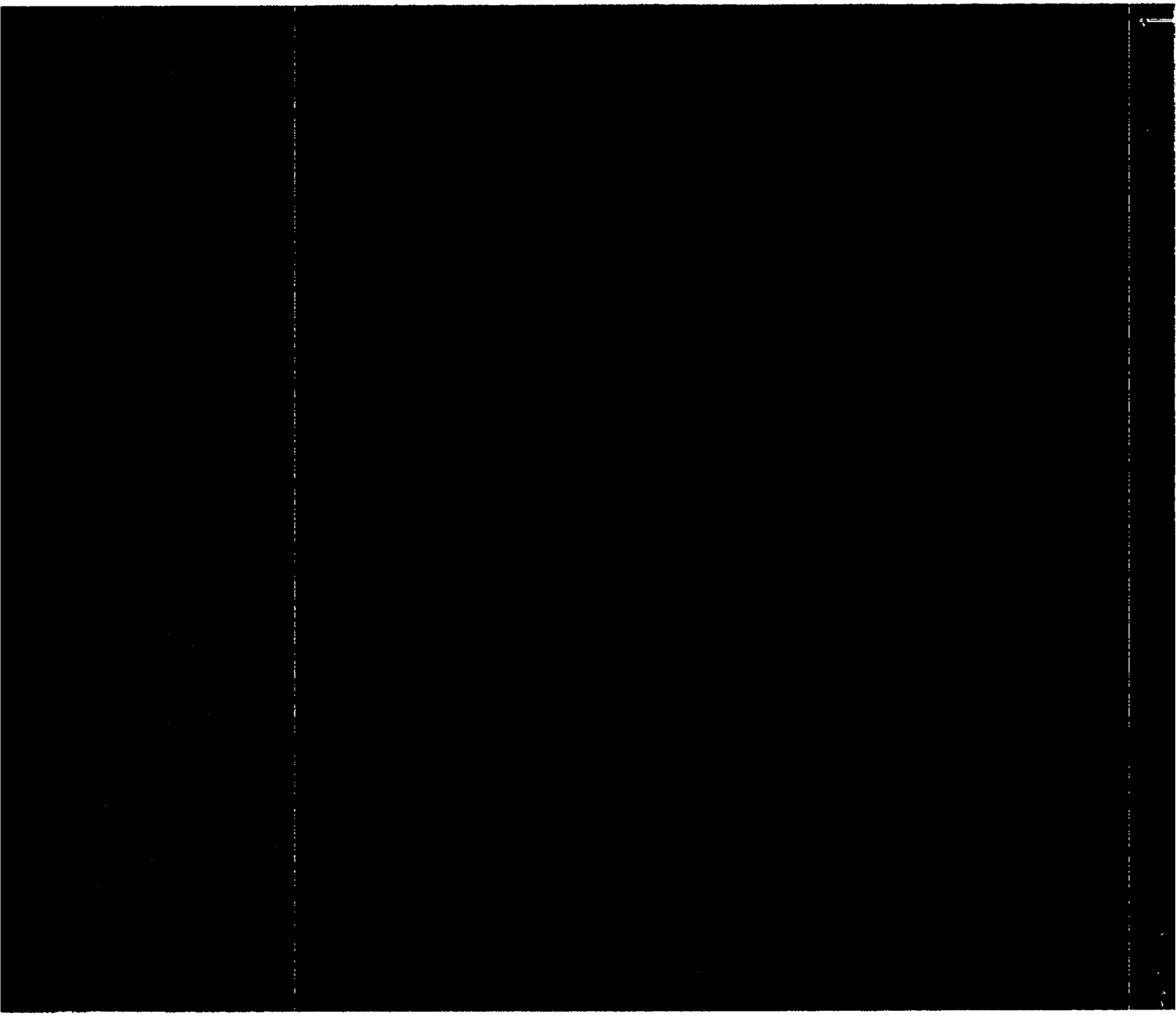

Los Alamos